J. Fluid Mech. (1993), *vol.* 252, *pp.* 79–98

Nonlinear analysis of buoyant convection in binary solidification with application to channel formation

By GUSTAV AMBERG[1] AND G. M. HOMSY[2]

[1] Department of Mechanics, Royal Institute of Technology, S-100 44 Stockholm, Sweden

[2] Department of Chemical Engineering, Stanford University, Stanford, CA 94305, USA

(Received 15 June 1992 and in revised form 7 January 1993)

We consider the problem of nonlinear thermal-solutal convection in the mushy zone accompanying unstable directional solidification of binary systems. Attention is focused on possible nonlinear mechanisms of chimney formation leading to the occurrence of freckles in solid castings, and in particular the coupling between the convection and the resulting porosity of the mush. We make analytical progress by considering the case of small growth Péclet number, δ, small departures from the eutectic point, and infinite Lewis number. Our linear stability results indicate a small $O(\delta)$ shift in the critical Darcy–Rayleigh number, in accord with previous analyses. We find that nonlinear two-dimensional rolls may be either sub- or supercritical, depending upon a single parameter combining the magnitude of the dependence of mush permeability on solids fraction and the variations in solids fraction owing to melting or freezing. A critical value of this combined parameter is given for the transition from supercritical to subcritical rolls. Three-dimensional hexagons are found to be transcritical, with branches corresponding to upflow and lower porosity in either the centres or boundaries of the cells. These general results are discussed in relation to experimental observations and are found to be in general qualitative agreement with them.

1. Introduction

The coupling between fluid flow and phase growth is important in many technological applications, including the casting of metals and crystallization of pure substances. Recent general reviews include Glicksman, Coriell & McFadden (1986) and Huppert (1990) among others. Of particular interest here is the case when the liquid is a chemical mixture that freezes with a composition different to that of the melt. This leads to compositional and temperature gradients that may be unstable, thus influencing the nature of the material when it is finally frozen. When an alloy is solidified, there is a primary instability marking the breakdown of simple one-dimensional growth. It is well known that a second mode of dendritic growth then occurs in which there is an appreciable two-phase region, referred to as a 'mush', in which solid dendrites and liquid coexist. A large number of experimental observations over the last 10–15 years have identified another, secondary, instability by which the mush becomes spatially non-uniform (see Chen & Chen 1991; Copley *et al.* 1970; Tait, Jahrling & Jaupart 1992; Tait & Jaupart 1992; Sample & Hellawell 1984; Sarazin & Hellawell 1988; and reference therein). It is this second instability that is of interest here. One of the consequences of this secondary instability is the formation of channels or chimneys of essentially pure liquid that are typically oriented in the direction of gravity. When finally frozen, the fossil record of these chimneys often manifests itself

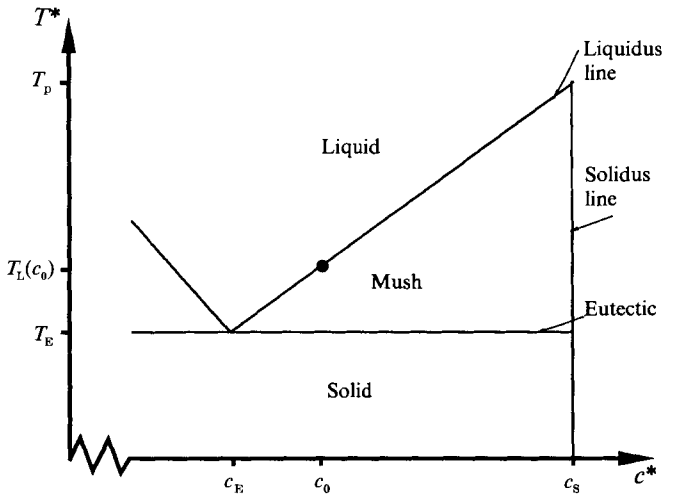

FIGURE 1. A schematic phase diagram. The features of this graph are similar to those of an ammonium chloride–water system, which is often used in experiments on chimney formation. The state of the fresh liquid at the top of the domain, $T^* = T_L(c_0)$, $c^* = c_0$ is indicated by a dot.

by localized regions of different chemical composition in the sample, known as 'freckles'. It has been speculated by many investigators that the origin of freckles is related to a buoyancy-driven instability in the mush by the following mechanism: during freezing from below, solute is rejected from the solid dendrites and is enriched in the interdendritic liquid. If the rejected constituent is lighter, as is frequently the case, the cold, solute rich liquid near the bottom is often lighter than the warmer liquid above. The liquid is thus unstably stratified and thermal-solutal convection may occur. Once convection has started an important coupling between the convection and the porosity of the mush becomes possible. The mush will attain a temperature, composition and solid fraction that is dictated by a combination of the local thermodynamic state and the phase diagram, leading to the possibility of either remelting or enhanced freezing of the solid. If the details are such that remelting occurs in regions of upflow, the local porosity will increase there, leading to a reduction in the viscous resistance to flow, and a positive feedback mechanism for further focusing of the upflow. This coupling between flow and temperature via the porosity is a very intricate mechanism that is thought to be responsible for the nucleation and growth of chimneys.

Solidification of binary systems are to a large extent governed by the phase diagram, i.e. relations between composition c^* and temperature T^* at the phase boundaries. A sketch of a representative phase diagram is shown in figure 1. The liquidus line $T_L(c^*)$ relates the composition of the liquid in the porous mush to the temperature. It has been assumed to be linear according to

$$T^* = T_L(c^*) = T_E + \Gamma(c^* - c_E), \tag{1.1}$$

where Γ is a constant (see figure 1). This relation is valid in the temperature range $T_E < T^* < T_p$. For temperatures above the melting temperature for pure material, T_p, no solid is formed regardless of composition. When the temperature falls below the eutectic temperature, T_E, all remaining liquid, which is then of composition c_E, solidifies immediately. Also, the solidus line is assumed to be vertical, i.e. the solids inside the mush are composed of pure solute ($c_s = 1$). These assumptions are somewhat restrictive, but are representative for the common model system ammonium

chloride–water. Our main conclusions will be relatively independent of this last assumption.

There have been only a few analyses that develop quantitative models to describe this process and the parameters on which it depends. Fowler (1985) was one of the first to pose and solve a linear instability model to couple buoyancy-drive convection with the resulting porosity of the mush. However, he made many restrictive assumptions that limit the applicability of the results. More recently, Worster (1992) solved a linear instability problem including the possible coupling between convection in the mush and in the liquid melt above the mush. His work is an important antecedent of ours, as he showed that there are two modes of convection associated with the density profiles in the mush and the melt, respectively, and that there is seldom any significant coupling between the two. Our model, developed below, focuses on the mode appropriate to convection in the mush.

In addition to these analyses of the linear stability problem, there have been recent attempts to understand chimney formation by direct numerical simulation of model partial differential equations in both two and three dimensions (see e.g. Felicelli, Heinrich & Poirier 1991; Neilson & Incropera 1993). While instructive, these studies often suffer from insufficient numerical resolution when the lateral scale of the chimney is commensurate with the grid size, and they do not allow dependence upon parameters to be identified.

We are interested in the problem of nonlinear convection and phase evolution in unstable dendritic growth. Linear stability theory predicts smooth periodic variations in porosity, with regions of upflow and downflow of the same size, while experiments and simulations show localized upflow regions. Tait & Jaupart (1992) and Worster (1992) have suggested on intuitive grounds that the bifurcation could be subcritical, since a convective flow would experience less flow resistance in a fully developed chimney than in an almost uniform mush.

In order to investigate this mechanism in more detail, we analyse a model problem appropriate for a binary system close to the eutectic composition. Weakly nonlinear theory is used to obtain information on the character of the bifurcation from the stagnant state. Both two-dimensional rolls and three-dimensional hexagonal patterns are investigated. This study complements the previous studies of the linear stability by providing information about possible hysteresis effects, subcritical instability, and illuminates the effect of focusing of a chimney by remelting. It is complementary to full numerical simulations of chimney formation by yielding the explicit dependencies of stability properties on the parameters of the problem. The main limitations of this study are that it is restricted to binary systems that are close to the eutectic composition in a non-dimensional sense, and that the free boundary at the top of the mush is not included. These are restrictions that may be relaxed in further studies.

The outline of the paper is as follows: in §2 the non-dimensional form of the governing equations is given and our 'close to eutectic' approximation is discussed. These equations are solved for small but finite disturbance amplitudes, using weakly nonlinear theory, in §3. The results and their implications for real chimney formation are discussed in §4.

2. Formulation

We consider a binary mixture that solidifies owing to cooling from below at conditions well beyond the primary instability so that the solid is growing dendritically, forming a mushy layer of infinite extent in the (x, y)-plane. Figure 2(a) sketches the

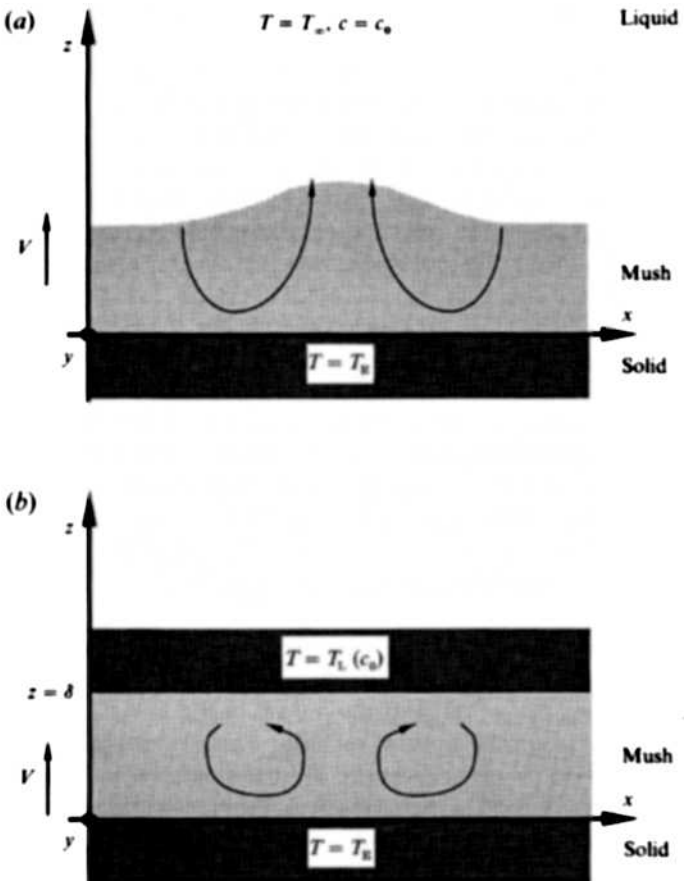

FIGURE 2. Two different geometries of the mushy layer. (*a*) Mush growing upwards into a basin of superheated liquid. The mush–liquid interface is a free surface. (*b*) Mush confined between two boundaries. The position of the upper edge of the mush is controlled by feeding liquid through a porous block at the liquidus temperature. The latter case is investigated here.

situation that might pertain in experiments such as those by Tait & Jaupart (1992) and Chen & Chen (1991), in which a mush propagates upwards into a deep bath of superheated mixture. The mush is then bounded at the top by a free interface. The mush/solid mixture freezes at a rate that is time-dependent, and limited by thermal diffusion within the mush (Huppert 1990). As explained above, we focus on instability modes present within the mush, and therefore adopt a simplified model geometry shown in figure 2(*b*). A mush is held between a solid lower boundary and a top interface, which are taken to be isothermal and fixed. The macroscopic solidification rate is taken to be constant and therefore in a frame moving with the solidification velocity V, liquid of composition c_0 is transferred through the upper boundary to replace the solids that are withdrawn at the bottom. The lower boundary is at the eutectic temperature, so that the mixture is completely solid at $z < 0$. The upper boundary is kept at the liquidus temperature of the mixture, and the entire space is assumed to be filled with a mush, which we model as a porous medium. While there are differences in the two situations, e.g. unconstrained growth is inherently time-dependent while our model has a steady base state, these are probably of secondary importance to the main objectives of our analysis.

The density of the liquid is assumed to vary linearly both with temperature and composition:

$$\rho = \rho_0[1-\alpha(T^*-T_E)+\beta(c^*-c_E)] = \rho_0(1+[(\beta/\Gamma)-\alpha](T^*-T_E)). \tag{2.1}$$

Γ is the slope of the liquidus curve and the liquidus relation (1.1) was used to eliminate the composition c^* in the last equality, leading to a Boussinesq approximation with effective expansion coefficient $[(\beta/\Gamma)-\alpha]$, which may become positive and lead to buoyancy-driven convection when the solutal effect dominates.

The equations governing the evolution of a porous mush have been given by Hills, Loper & Roberts (1983), and have been studied in different contexts by several authors. Here we will start with a non-dimensional form very similar to that used by Worster (1992):

$$0 = -\nabla p - K(\phi)\,\boldsymbol{u} - Ra\,\theta \boldsymbol{e}_z, \tag{2.2a}$$

$$\nabla\cdot\boldsymbol{u} = 0, \tag{2.2b}$$

$$-\frac{\partial}{\partial z'}[C\phi+(1-\phi)\,\theta]+\nabla\cdot(\theta\boldsymbol{u}) = \frac{1}{Le}\nabla^2\theta, \tag{2.2c}$$

$$-\frac{\partial\theta}{\partial z'}+\nabla\cdot(\theta\boldsymbol{u}) = \nabla^2\theta - St\frac{\partial\phi}{\partial z'}. \tag{2.2d}$$

The dependent variables are velocity and pressure, $\boldsymbol{u}$ and p, temperature θ, and the volume fraction solid in the mush, ϕ ($= 1-\chi$ where χ denotes the porosity). Equation (2.2*a*) is the Darcy–Boussinesq equation. With the assumption that the densities of the solid and liquid are equal (no solidification shrinkage), mass conservation is described by equation (2.2*b*). Equation (2.2*c*) is derived from conservation of solute, assuming that the liquid composition is approximately uniform over microscopic distances corresponding to the dendrite spacing, i.e. that a Péclet number based on mass diffusivity and microscopic lengthscale is less than unity. The non-dimensional form of the liquidus relation (1.1) ($c = \theta$) has been used to replace solute concentration by non-dimensional temperature. The assumption that dendrites are composed of pure solute is also used. The last equation, (2.2*d*), expresses the conservation of heat, in which the effective thermal conductivity of the mush is taken to be independent of porosity. In using this equation, it is assumed that a thermal Péclet number based on the microscopic lengthscale is less than unity, so that the microscopic transport is conductive in nature.

The factor $K(\phi)$ in (2.2*a*) accounts for the variation of permeability with solid fraction:

$$K(\phi) = \Pi(0)/\Pi(\phi).$$

$\Pi(\phi)$ is the permeability as a function of solid fraction. We will follow Worster (1992) in choosing a form for $\Pi(\phi)$ that tends to a finite value as ϕ tends to zero, so that the reference value $\Pi(0)$ is well defined. The particular form of $K(\phi)$ will be specified later.

Equations (2.2) have been made dimensionless using the following scales (* denotes dimensional quantities):

$$\theta = \frac{T^*-T_L(c_0)}{T_L(c_0)-T_E}, \tag{2.3a}$$

$$\boldsymbol{u} = \boldsymbol{u}^*/V, \tag{2.3b}$$

$$p = p^*/(\kappa\mu/\Pi(0)), \tag{2.3c}$$

$$(x', y', z') = (x^*, y^*, z^*)/H. \tag{2.3d}$$

Here, $T_L(c_0)$ is the liquidus temperature at the original composition c_0, T_E is the eutectic temperature at which the mush becomes completely solid (see figure 1). κ and μ are the heat diffusivity (defined as the effective thermal conductivity of the mush divided by the volumetric heat capacity of the fluid) and the dynamic viscosity respectively, and $H = \kappa/V$ is a characteristic length.

Five non-dimensional numbers appear:

$$Ra = \frac{g[T_L(c_0) - T_E](\beta/\Gamma - \alpha) H\Pi(0)}{\kappa\nu}, \tag{2.4a}$$

$$C = \frac{T_p - T_L(c_0)}{T_L(c_0) - T_E} = \frac{c_s - c_0}{c_0 - c_E}, \tag{2.4b}$$

$$St = \frac{L}{C_p(T_L(c_0) - T_E)}, \tag{2.4c}$$

$$Le = \frac{\kappa}{D}, \tag{2.4d}$$

$$\delta = d/H = \frac{dV}{\kappa}. \tag{2.4e}$$

The first of these is the mush Rayleigh number, as commonly used in studies of chimney formation, defined using the effective expansion coefficient, $(\beta/\Gamma - \alpha)$. C is a concentration ratio used by Worster (1992), which expresses important features of the phase diagram. Note that C will become large if the initial composition c_0 is close to the eutectic composition c_E. St is a Stefan number expressing the importance of latent heat *vs.* specific heat release. Le is the Lewis number, which will always be large, typically $Le > 100$ (at least). The last parameter δ, a growth Péclet number, does not appear in the equations themselves, but will appear in the boundary conditions. It denotes the ratio between the actual height of the domain d and the lengthscale $H = \kappa/V$ which has been used in the non-dimensionalization. The usual Darcy–Rayleigh number commonly used in the study of convection in porous media is $Ra_D = Ra\delta$. Below, we will assume δ to be small, C to be large, $\approx 1/\delta$, and solutions will be derived as asymptotic expansions in δ.

The eutectic front at the bottom boundary is assumed to be translating upwards at a speed V. The upper boundary is thought to be the surface of a porous block through which mixture with composition c_0 is fed. The temperature of the porous block is controlled so that the liquid issuing at its lower surface is at the liquidus temperature $T_L(c_0)$ (see figure 2*b*).

The boundary conditions expressing these conditions are, in the x', y', z' frame that translates with the eutectic front:

$$\text{at} \quad z' = 0: \quad w = 0, \quad \theta = -1, \tag{2.5a}$$

$$\text{at} \quad z' = \delta: \quad w = 0, \quad \theta = 0, \quad \phi = 0. \tag{2.5b}$$

The parameter δ defined in (2.4*e*) appears here as the non-dimensional height of the mush. w is the z-component of the velocity $\boldsymbol{u}$.

Thus our model describes buoyancy-driven convection in a porous medium with constant through-flow at the boundaries. There is heat release but no volume change

on freezing and local thermodynamic equilibrium is assumed so that the composition and temperature are linked through the phase diagram. The permeability of the mush is dependent on the local porosity, which in turn depends upon the local composition and temperature, leading to an important feedback between changes in thermodynamic state, porosity, and flow resistance. We ignore complications associated with a free surface, while correctly capturing the important instability mechanism related to the flow in the interior of the mush. As we commented in the introduction, Worster (1992) identified two distinctly different linearly unstable modes, one associated with a thin layer of unstably stratified liquid above the mush–liquid interface, the other with the unstable stratification within the mush. With the present model, coupling between flow and remelting is described correctly for the nonlinear interior mode, which is the one thought to evolve into chimneys.

Our model also involves a choice of boundary conditions. An alternative boundary condition is $p = 0$ at $z' = \delta$, as studied in a different context by Wooding (1960). This would allow in- and outflow at the top boundary and may give closer quantitative agreement with results for a mush growing in a large bath. But this is expected to lead to quantitative rather than mechanistic differences between models, and may be the topic of further investigations.

The complete system (2.2) is quite complicated, even without a free upper boundary. Here we construct a weakly nonlinear solution, as we wish to derive analytical rather than numerical solutions, to be able to see parameter dependencies and identify mechanisms explicitly. For this to be possible, simplifications must be made. By studying a limit where the binary system is close to the eutectic composition ($C \gg 1$), and the mush height is much less than the diffusive lengthscale ($\delta \ll 1$), a suitable approximate system can be derived. When $\delta \ll 1$, the base state temperature will be approximately linear, which means that the lowest-order approximate form of (2.2*d*) will have constant coefficients. Similarly, for $C \gg 1$, the base state solid fraction will be small and $K(\phi) = 1 + O(\phi)$, so that (2.2*a*) will have constant coefficients to lowest order.

An approximation similar to this has been used by Fowler (1985) to study possible linear stability mechanisms leading to convective flow and freckles. His scaling is somewhat different though, as it leads to a lowest-order heat equation (2.2*c*) where the coupling between temperature and velocity has been lost. Instead he includes the free surface of the mush and uses an approximate boundary condition at the interface, which provides the coupling between temperature and velocity.

The particular asymptotic limit that we are looking at here is defined by letting $\delta \to 0$, while $C_s = \delta C = O(1)$ and $St = O(1)$. In addition, we treat the case $Le = \infty$, corresponding to neglecting mass diffusion. Worster (1992) has shown that the effect of this approximation is to suppress the 'boundary layer mode', i.e. the onset of convection in a thin layer of liquid just above the mush–liquid interface. The onset of the convective mode internal to the mush is not affected to any great extent by these approximations.

The amplitude of convection, ϵ, is the other small parameter in the problem and will be assumed to be $O(\delta)$, i.e. $\epsilon/\delta = A = O(1)$. This assumption is motivated by the expectation that the base state solid fraction will be $O(\delta)$, while the finite-amplitude disturbance will be $O(\epsilon)$. Thus, the assumption $\epsilon \sim \delta$ includes the interesting situation when the base state solid fraction is altered significantly by the nonlinear contribution. ϵ could not be significantly larger than δ, since the finite amplitude contribution would then most probably cause ϕ to become negative, in which case the equations (2.2) are not valid. Conversely, $\epsilon \ll \delta$ would rule out the interesting effects. Taking $\epsilon \sim \delta$ and

analysing the dominant balances in the equations for the limit above shows that the problem should be rescaled as follows:

$$\theta = \theta_B(z) + \epsilon\hat{\theta}(x, y, z), \tag{2.6a}$$

$$\boldsymbol{u} = R\frac{\epsilon}{\delta}\hat{\boldsymbol{u}}(x, y, z), \tag{2.6b}$$

$$p = Rp_B(z) + R\epsilon\hat{p}(x, y, z), \tag{2.6c}$$

$$\phi = \delta\phi_B(z) + \epsilon\hat{\phi}(x, y, z), \tag{2.6d}$$

$$(x', y', z') = \delta(x, y, z), \tag{2.6e}$$

$$R^2 = \delta Ra = Ra_D. \tag{2.6f}$$

The subscript B denotes the base-state solution, and the ^-variables are the two- or three-dimensional disturbances. The lengthscale is now, as expressed in (2.6*e*), the height of the gap instead of the diffusive length. A consequence of this is that the relevant Rayleigh number should be redefined using the new lengthscale. In order to express the equations in self-adjoint form, R, the square root of Ra_D, has been introduced in both equation (2.6*f*), and the rescaled velocity and pressure.

By introducing these expressions in equations (2.2), and setting $1/Le = \epsilon = 0$, equations for the base state, $\theta_B(z)$, $\phi_B(z)$, $p_B(z)$ result, where prime denotes differentiation with respect to z:

$$0 = -p_B' + R\theta_B, \tag{2.7a}$$

$$-C_s\phi_B' - \theta_B' + \delta(\phi_B\theta_B)' = 0, \tag{2.7b}$$

$$-\delta\theta_B' - \theta_B'' - \delta^2 St\,\phi_B' = 0. \tag{2.7c}$$

The boundary conditions on the base state are:

$$\text{at} \quad z = 0: \quad \theta_B = -1, \tag{2.8a}$$

$$\text{at} \quad z = 1: \quad \theta_B = 0, \quad \phi_B = 0. \tag{2.8b}$$

The steady base state in this limit can be easily found from (2.7). Since the finite-amplitude solution will be obtained as a series expansion in δ, it is convenient to express the base state in its expansion as well:

$$\theta_B(z) = \theta_{B1}(z) + \delta\theta_{B2}(z) + \delta^2\theta_{B3}(z) + O(\delta^3),$$
$$\phi_B(z) = \phi_{B1}(z) + \delta\phi_{B2}(z) + \delta^2\phi_{B3}(z) + O(\delta^3).$$

The result is:

$$\theta_B(z) = -(1-z) + \delta\tfrac{1}{2}z(1-z) + \delta^2\left(\tfrac{1}{12}z(z-1)(2z-1) + \frac{St}{2C_s}z(1-z)\right) + O(\delta^3), \tag{2.9a}$$

$$\phi_B(z) = \frac{1-z}{C_s} + \delta\left(-\frac{1}{2C_s}z(1-z) - \frac{1}{2C_s^2}(1-z)^2\right)$$
$$+ \delta^2\left(-\frac{z}{12C_s}(z-1)(2z-1) + \frac{1}{C_s^2}[(z-1)^2 + \tfrac{1}{2}St\,z(z-1)] + \frac{1}{C_s^3}(1-z)^3\right) + O(\delta^3). \tag{2.9b}$$

Note that both θ_B and ϕ_B are linear in z to lowest order. A finite growth Péclet number leads to a convective–diffusive balance and a compaction of the isodensity surfaces

near the bottom boundary, or equivalently, to a density profile that is no longer linear. Also, according to (2.6*d*), the base state solid fraction ϕ is $O(\delta/C_s) \ll 1$ to lowest order, as expected. The parameter C_s gives the magnitude of the porosity variation due to variations in temperature (and therefore concentration) and will play a central role in determining the nature of the bifurcation.

The equations for the disturbances are obtained by introducing (2.6) with $\epsilon \neq 0$ in (2.2) and making use of (2.7):

$$0 = -\nabla\hat{p} - K(\delta\phi_B + \epsilon\hat{\phi})\,\hat{\boldsymbol{u}} - R\hat{\theta}\boldsymbol{e}_z, \tag{2.10a}$$

$$\nabla\cdot\hat{\boldsymbol{u}} = 0, \tag{2.10b}$$

$$-C_s\frac{\partial\hat{\phi}}{\partial z} + R\theta_B'\hat{w} - \delta\frac{\partial\hat{\theta}}{\partial z} + \frac{\partial}{\partial z}[\delta\theta_B\hat{\phi} + \delta^2\phi_B\hat{\theta} + \epsilon\delta\hat{\phi}\hat{\theta}] + \epsilon R\nabla\cdot(\hat{\theta}\hat{\boldsymbol{u}}) = 0, \tag{2.10c}$$

$$\nabla^2\hat{\theta} - R\theta_B'\hat{w} = -\delta\frac{\partial\hat{\theta}}{\partial z} + \epsilon R\nabla\cdot(\hat{\theta}\hat{\boldsymbol{u}}) + \delta St\frac{\partial\hat{\phi}}{\partial z}. \tag{2.10d}$$

Since $\phi = O(\delta)$ is expected to be small, according to (2.6*d*), we expand the coefficient $K(\phi)$ which contains the information on how the permeability varies with solid fraction as a series in ϕ:

$$K(\phi) = 1 + K_1\phi + K_2\phi^2 + O(\phi^3). \tag{2.11}$$

K_1 and K_2 are constants whose numerical values will be specified later.

3. Solution

The equations for the disturbances (2.10) are solved using standard methods for bifurcation problems (Iooss & Joseph 1980; Palm, Weber & Kvernvold 1972; Busse 1967). This has been carried out using the symbolic computation system Maple V (Char *et al.* 1991). Since the solution procedure follows standard lines and the expressions become increasingly complicated at higher order, it is only outlined here.

The dependent disturbance variables and the controlling parameter R are all assumed to have regular expansions in the amplitude ϵ.

$$\hat{\theta}(x,y,z) = \theta_1(x,y,z) + \epsilon\theta_2(x,y,z) + \epsilon^2\theta_3(x,y,z) + O(\epsilon^3), \tag{3.1a}$$

$$\hat{\boldsymbol{u}}(x,y,z) = \boldsymbol{u}_1(x,y,z) + \epsilon\boldsymbol{u}_2(x,y,z) + \epsilon^2\boldsymbol{u}_3(x,y,z) + O(\epsilon^3), \tag{3.1b}$$

$$\hat{\phi}(x,y,z) = \phi_1(x,y,z) + \epsilon\phi_2(x,y,z) + \epsilon^2\phi_3(x,y,z) + O(\epsilon^3), \tag{3.1c}$$

$$R = R_0 + \epsilon R_1 + \epsilon^2 R_2 + O(\epsilon^3). \tag{3.1d}$$

Equations (2.10) contain two different small parameters, ϵ and δ. As explained above, it is reasonable to assume that $\delta = \epsilon/A$, where $A = O(1)$. The equations (2.10) then contain the small parameter ϵ, and the $O(1)$ quantities A, St, C_s, and from (2.11), K_1 and K_2. Introducing the expansions and collecting equal powers of ϵ, equations of the following form are obtained (after eliminating u, v and pressure, leaving θ_k, ϕ_k and the z-component w_k of $\boldsymbol{u}_k = (u_k, v_k, w_k)$):

$$\nabla^2 w_k + R_0\nabla_2^2\theta_k = F_k, \tag{3.2a}$$

$$\nabla^2\theta_k - R_0 w_k = G_k, \tag{3.2b}$$

$$-C_s\frac{\partial\phi_k}{\partial z} + R_0 w_k = H_k, \tag{3.2c}$$

with the boundary conditions:

$$\theta_k = w_k = 0 \quad \text{at } z = 0, 1; \quad \phi_k = 0 \quad \text{at } z = 1.$$

Here $k = 1, 2, 3 \ldots$, and ∇_2^2 denotes the two-dimensional Laplacian $(\partial^2/\partial x^2 + \partial^2/\partial y^2)$. The right-hand sides F_k, G_k, H_k are nonlinear functions of the lower-order solutions and the parameters, i.e. they depend on w_n, θ_n, ϕ_n with $n < k$, as well as A, St, C_s, K_1, K_2, and the lower-order coefficients R_n, $n \leqslant k$. The lowest-order problem corresponds to the linear stability problem for which the right-hand sides vanish, i.e. $F_1 = G_1 = H_1 = 0$. Equations (3.2*a*) and (3.2*b*) constitute a self-adjoint eigenvalue problem for the eigenvalue R_0 with eigenfunctions w_1, θ_1. The solid fraction ϕ_1 is then obtained from equation (3.2*c*).

Following standard bifurcation analysis, the next order coefficient in the expansion of R, R_1, is obtained from a solvability condition. This is obtained by projecting the right-hand sides of the second-order equation onto the first order eigenmode. This results in a scalar equation for R_1. For this particular value of R_1, the non-homogeneous second-order equations, (3.2) with $k = 2$, may be solved for w_2, θ_2, ϕ_2, and the process may be continued through higher orders. Here we have not carried this further than obtaining R_2.

We first consider two-dimensional solutions corresponding to the initial onset of convection in the form of rolls. Such a solution is relevant to experiments such as those of Chen & Chen (1991) that use 'Hele-Shaw' geometries of crystallization between closely placed plates. The effect of nearby sidewalls is to suppress any variation in the third dimension. Assuming that the lowest-order solution is two-dimensional, independent of y, and with a sinusoidal variation with x, the following expressions are obtained:

$$w_1 = \pi \sin(\pi z)\cos(\pi x), \tag{3.3a}$$

$$\theta_1 = -\sin(\pi z)\cos(\pi x), \tag{3.3b}$$

$$\phi_1 = -\frac{2\pi}{C_s}[\cos(\pi z) + 1]\cos(\pi x), \tag{3.3c}$$

$$R_0 = 2\pi. \tag{3.3d}$$

These solutions are identical to those for two-dimensional convective rolls in a passive porous medium, Palm *et al.* (1972). The numerical value of R_0 is obtained in the usual way by minimizing R_0 with respect to the wavenumber in the x-direction. As is well-known, the minimum occurs for wavenumber $k = \pi$.

Application of the solvability condition for the second-order equations as outlined above yields an expression for R_1:

$$R_1 = \frac{R_{1\delta}}{A} = \frac{\pi(K_1 - 2St)}{2AC_s}. \tag{3.4}$$

Using this value for R_1, the second-order equations can be solved for w_2, θ_2, ϕ_2. Owing to the nonlinearity they will now contain terms proportional to $\sin(2\pi x)$ and $\cos(2\pi x)$, i.e. with a wavenumber in the x-direction which is twice that of the first-order solutions. The full expressions are rather complicated and are not reproduced here. Applying the solvability condition to the third-order equations yields the next term in the expansion of R:

$$R_2 = \frac{1}{A^2}R_{2\delta} + R_{2\epsilon}, \tag{3.5a}$$

a	0.7288876652
b	2.844035870
c	0.2322439175
d	0.7853981631
e	0.1110053260
f	2.356194490
g	0.3568249580
h	15.50313834
k	82.68340448
l	85.26726084
m	7.751569171

TABLE 1. The numerical constants in the expression for R_2

where

$$R_{2\delta} = \frac{1}{C_s^2}[-cK_1^2 + a(K_2 - K_1) - gC_s K_1 - d\,St\,K_1 + b\,St + f\,St^2 + e\,C_s^2], \tag{3.5b}$$

$$R_{2\epsilon} = \frac{1}{C_s^2}(-h\,C_s K_1 - kK_1^2 + lK_2 + mC_s^2). \tag{3.5c}$$

Here a–h, k–m are positive pure numbers given in table 1. Replacing A by its definition ϵ/δ, the complete expression for R to this order is:

$$R = 2\pi + \delta\frac{\pi(K_1 - 2St)}{2C_s} + \delta^2 R_{2\delta} + \epsilon^2 R_{2\epsilon} + O(\epsilon^3). \tag{3.6}$$

Here R and δ are known parameters. The $O(\delta)$ and $O(\delta^2)$ terms represent small shifts in the critical Rayleigh number owing to the coupling between flow and temperature through the dependency of permeability on solid fraction, and the release of latent heat. The $O(\epsilon^2)$ term represents the change in R required to obtain a given finite amplitude ϵ. This does not depend on St, i.e. the release of latent heat, but only on K_1 and K_2, the form of the permeability function, and the concentration ratio C_s. Given R and δ, (3.6) determines the amplitude ϵ of the disturbance. Since there is no term linear in ϵ, the amplitude of convection will be proportional to

$$\epsilon = \pm\left(\frac{R - R_{\text{lin}}}{R_{2\epsilon}}\right)^{\frac{1}{2}}, \tag{3.7}$$

where R_{lin} denotes the three first terms in the expansion of R. The sign of $R_{2\epsilon}$ now determines whether the steady finite-amplitude solution exists for values of R above or below R_{lin}. It will be seen in the next section that for typical cases $R_{2\epsilon}$ is negative, and the solution exists for $R < R_{\text{lin}}$, i.e. bifurcation from the stagnant state is subcritical.

These results can be checked in two ways. First, by putting $\delta = 0$, $K_1 = K_2 = 0$, equations (2.7) and (2.10) reduce to those studied by Palm *et al.* (1972). The expression (3.6) becomes $R = 2\pi + \epsilon^2\pi^3/4$, which agrees with the results of Palm *et al.* Secondly, Homsy & Sherwood (1976) calculated the onset of instability for a porous medium with through flow. The same problem is obtained here if $\epsilon = 0$, $K_1 = K_2 = St = 0$. Equation (3.6) then becomes $R = 2\pi + 0.1110053260\delta^2$. This is in good agreement with the results of Homsy & Sherwood, even though a very detailed comparison is not possible since their results were only presented graphically.

The solutions obtained above assume that the finite-amplitude solutions are two-dimensional rolls. The more general case of three-dimensional convection is now considered, as it is relevant to experiments in containers with $O(1)$ aspect ratios in the plane perpendicular to the growth direction. It is well known that rolls will still be preferred if the equations are self-adjoint. However for slightly non-self-adjoint systems, such as non-Boussinesq fluids, hexagonal cells become possible (Busse 1967). Since our problem is self-adjoint only in the limit of $\delta = 0$, three-dimensional hexagonal cell solutions are possible at finite-growth Péclet number. The first-order eigenfunctions corresponding to hexagons are obtained as superpositions of the two-dimensional eigenmodes given above, each term rotated 120° in the (x, y)-plane. The result is as follows:

$$w_1 = \pi \sin(\pi z)\, \eta(x, y), \tag{3.8a}$$

$$\theta_1 = -\sin(\pi z)\, \eta(x, y), \tag{3.8b}$$

$$\phi_1 = -\frac{2\pi}{C_s}(\cos(\pi z) + 1)\, \eta(x, y), \tag{3.8c}$$

where

$$\eta(x, y) = \cos(\pi y) + \cos[\tfrac{1}{2}\pi(x3^{\frac{1}{2}} + y)] + \cos[\tfrac{1}{2}\pi(x3^{\frac{1}{2}} - y)].$$

The solution then proceeds as in the two-dimensional case, but the solvability condition for the second-order equations now gives a different expression for R_1:

$$R_1 = \frac{1}{A} R_{1\delta} + R_{1\epsilon}, \tag{3.9}$$

where

$$R_{1\delta} = \frac{\pi(K_1 - 2St)}{2AC_s},$$

$$R_{1\epsilon} = -(\tfrac{136}{9} + \tfrac{3}{2}\pi^2)\frac{K_1}{C_s}.$$

The complete expression for R is then:

$$R = 2\pi + \delta R_{1\delta} + \epsilon R_{1\epsilon} = 2\pi + \delta\frac{\pi(K_1 - 2St)}{2C_s} - \epsilon(\tfrac{136}{9} + \tfrac{3}{2}\pi^2)\frac{K_1}{C_s} + O(\epsilon^2). \tag{3.10}$$

The first two terms determine the critical value R_{lin} of R for linear stability, which through $O(\delta)$ is identical to the shift in critical Rayleigh number for rolls. The last term is now linear in ϵ, so for hexagons the amplitude varies linearly with R:

$$\epsilon = \frac{R - R_{\text{lin}}}{R_{1\epsilon}}, \tag{3.11}$$

where $R_{1\epsilon}$ is the second of the two terms in R_1. $R_{1\epsilon}$ is negative, so ϵ is positive for $R < R_{\text{lin}}$, and negative for $R > R_{\text{lin}}$. By examining the solution for w_1, we see that positive $\epsilon(R < R_{\text{lin}})$ correspond to upflow at the centre of a hexagonal cell, while negative $\epsilon(R > R_{\text{lin}})$ corresponds to upflow around the rim of the hexagon.

4. Discussion

The solutions in (3.3), (3.6), (3.8), (3.10) (and also the second-order corrections that have not been reproduced) are known as functions of the parameters δ, ϵ, C_s, St, K_1 and K_2. ϵ is calculated from Ra according to (2.6f) and (3.7) or (3.11). δ, C_s and St are

determined by the thermal boundary conditions and the properties of the binary mixture. K_1 and K_2 characterize the dependence of permeability on solid fraction, according to (2.11). For the permeability model used by Worster (1992),

$$K(\phi) = \Pi(0)/\Pi(\phi) = 1/(1-\phi)^3 = 1+3\phi+6\phi^2+O(\phi^3), \tag{4.1}$$

the values are $K_1 = 3$, $K_2 = 6$. These numbers will be used when discussing the general properties of the solution. Other micromechanical models for the resistance function $K(\phi)$, e.g. those corresponding to flow past periodic arrays of particles or along axes of cylinders as discussed in the appendix of Felicelli *et al.* (1991) give similar numerical values for K_1, K_2.

4.1. *Two-dimensional convection*

We first consider two-dimensional convection, such as occurs in Hele-Shaw geometries. Setting $\epsilon = 0$ in (3.6) recovers results from linear theory. This gives the same qualitative trends that were found by Homsy & Sherwood (1976) and Worster (1992): $Ra = R^2/\delta$ increases with decreasing δ, decreases with increasing $C(= C_s/\delta)$, and slowly decreases with St. A direct quantitative comparison with Worster is not possible, however, since the boundary conditions are different here, and also since Worster presented results for varying one of the three parameters $\theta_\infty \approx 1/\delta$, C and St, setting the remaining two to unity, while (3.6) is valid only for both θ_∞ and C greater than one.

The main result in (3.6) is the finite-amplitude term $\epsilon^2 R_{2\epsilon}$. In particular the sign of $R_{2\epsilon}$ is important, as it determines whether the onset of convection is subcritical or supercritical. As seen from (3.5*c*), $R_{2\epsilon}$ consists of four terms. The last term is positive and constant. The first two are negative, proportional to K_1/C_s and $(K_1/C_s)^2$, respectively. The third has the same sign as K_2. If the variation of permeability with solid fraction is negligible, K_1 and K_2 are zero. This makes $R_{2\epsilon} = m = \frac{1}{4}\pi^3 > 0$ and the bifurcation is supercritical, as is well known to be the case for convection in a passive porous medium (Palm *et al.* 1972). K_1 is positive if the permeability increases with decreasing solid fraction, as expected. Both the contributions involving K_1 are then negative, thus making the bifurcation subcritical for large enough values of K_1. The term proportional to K_2 is associated with curvature in the $K(\phi)$ relation, and is usually positive, decreasing the tendency towards subcritical bifurcation. For a positive value of K_2, the permeability increases less rapidly with decreasing solid fraction at values of ϕ below the base state value, than would be calculated for a linear $K(\phi)$ relation. Thus for $K_2 > 0$, the third term corrects for an overestimated permeability increase in the critical upflow regions with lowered values of ϕ.

Neglecting the curvature in the $K(\phi)$ relation allows further insight into the controlling mechanism for subcritical bifurcation. In this case, $R_{2\epsilon}$ depends only on the *combined* parameter, K_1/C_s. It is easy to see why this is the case, since it is a combination of the dependence of permeability on porosity and the magnitude of porosity changes with temperature that matters, not these effects taken separately. The value of K_1/C_s for which $R_2\epsilon = 0$, giving the transition from supercritical to subcritical rolls is easily calculated to be ≈ 0.226. If K_1/C_s is greater than this, $R_{2\epsilon}$ is negative and the bifurcation is subcritical. The mechanism is as anticipated: a fluctuation leading to a local upwelling of fluid results in a packet of fluid which is colder but more lean in the solute than its surroundings. As a result of the relatively higher thermal diffusivity, this packet equilibrates in temperature much faster than in composition. The fluid then appears to be superheated and accommodates to the constraint of local equilibrium by dissolving some solid. Thus we anticipate the formation of chimneys in upflow and a slow downward percolation of fluid through the remainder of the domain. Some of these features may be further understood through an examination of the solutions.

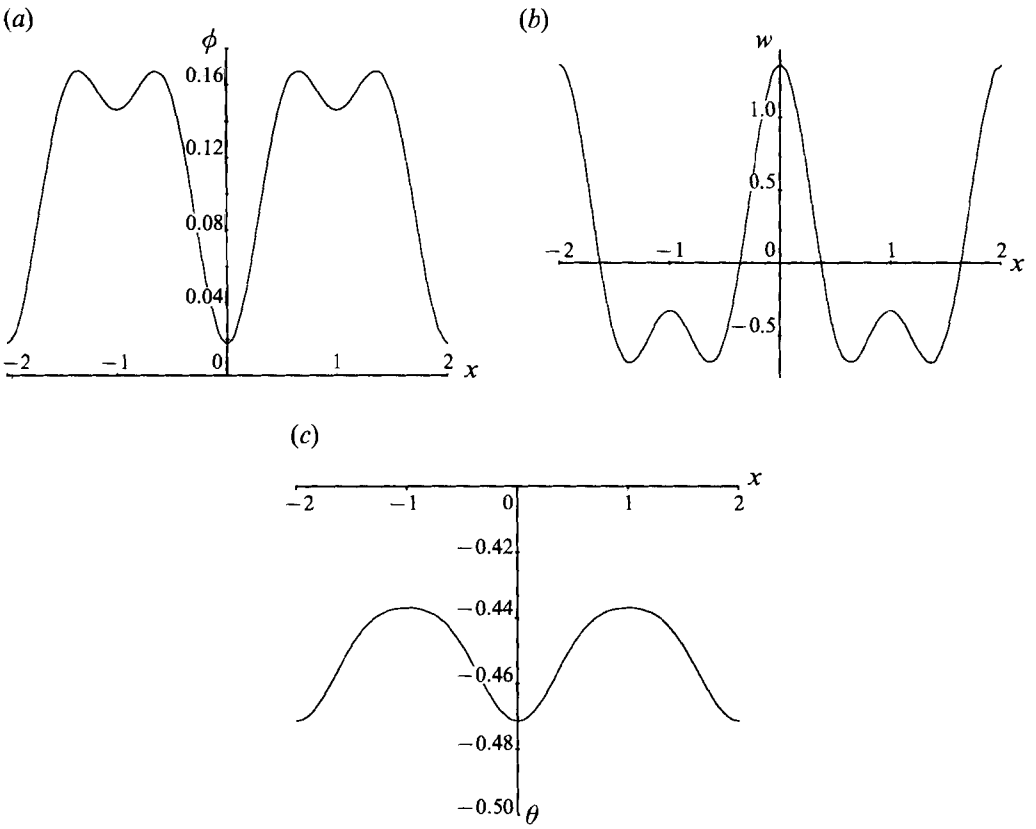

FIGURE 3. The finite-amplitude solution for a particular case with $\delta = 0.3$, $C_s = 1$, $St = 1$, $\epsilon = 0.015$. (*a*) The solid fraction ϕ as a function of x at $z = \frac{1}{2}$. The base state value of ϕ is 0.141. (*b*) The vertical velocity w as a function of x at $z = \frac{1}{2}$. (*c*) The temperature θ as a function of x at $z = \frac{1}{2}$. The temperature is -0.4513 in the base state.

The solutions were evaluated for a representative case with $\delta = 0.3$, $C_s = 1$, $St = 1$ and $\epsilon = 0.015$. (Although this solution is subcritical and is probably unstable – see discussion below – its structure is of interest here.) This value of ϵ corresponds to a value of R which is only 0.061 less than the critical value 6.93 for linear stability ($Ra_D = \delta Ra$ is 0.767 less than critical) and was chosen to make the minimum value of the porosity close to zero corresponding to an open channel. In figure 3, ϕ, w, θ have been drawn as functions of x in the interval $-2 < x < 2$, at the centre of the mush, $z = \frac{1}{2}$. The solutions extend periodically to $\pm\infty$. For these parameter values, the base state temperature is $\theta = -0.4513$ at $z = \frac{1}{2}$, and the base state solid fraction is $\phi = 0.141$. The expected localization of the regions with low solid fraction is indeed visible in figure 3(*a*), which shows rather narrow regions of low values of ϕ at $x = 0, \pm 2$. Note that it is consistent with the assumptions in the perturbation expansion for the perturbation in ϕ to be the same order of magnitude as the base state value of ϕ, see equation (2.6*d*). Comparing figures 3(*a*) and 3(*b*), it is seen that the region of low solid fraction does indeed correspond to a region of rising liquid, which is similarly localized. The maximum value for w is greater than one, which implies that the maximum dimensional liquid velocity is larger than V, the translating speed of the system. Figure 3(*c*) shows that the disturbance of the temperature field is quite weak, with a slightly lower temperature in the region where cold liquid rises.

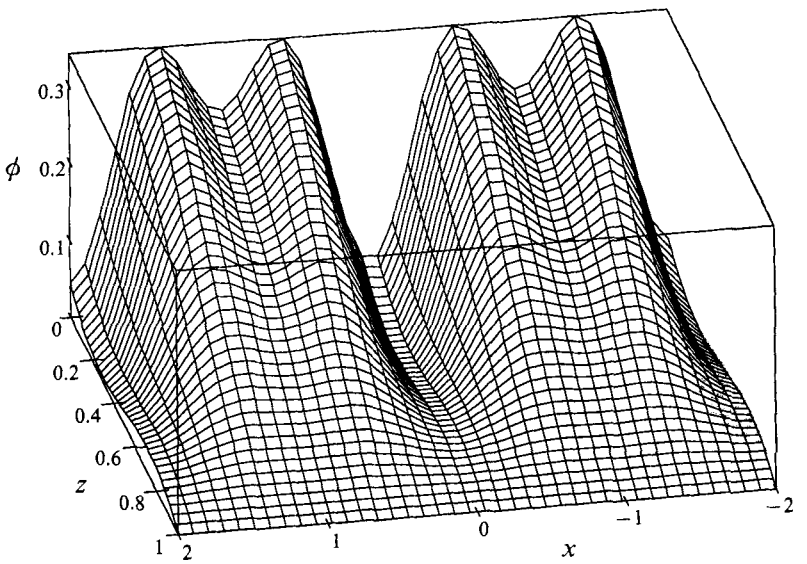

FIGURE 4. The solid fraction ϕ as a function of both x and z for the parameter values in figure 3. The warm boundary is at $z = 1$, the cold boundary at $z = 0$.

Figure 4 shows a three-dimensional plot of the solid fraction as a function of both x and z for the same case. In the downflow regions around $x = \pm 1$, the solid fraction is seen to increase more or less linearly away from the upper boundary ($z = 1$). In the upflow regions near $x = 0$, ϕ is close to zero over the entire depth. The general shape of the low solid fraction region in figure 4 resembles the pictures of fully developed chimneys obtained by Chen & Chen (1991) by computer tomography. They showed chimneys that extended all the way to the bottom plate, with little or no decrease in diameter. Their pictures also seem to suggest that the solid fraction is increased close to the chimney, something that has been predicted theoretically by Worster (1991).

In this example the value of ϵ was chosen to be 0.015, which makes the minimum value of ϕ almost zero, i.e. ϵ is close to the maximum allowable amplitude for these parameter values. This amplitude $\epsilon_{\max}$ can be estimated by solving $\phi = 0$ for $\epsilon = \epsilon_{\max}$, using (2.6*b*), (3.3*c*), (3.1*c*), (2.9*b*), discarding all higher-order terms for simplicity and noting that the minimum of ϕ is attained near $z = 0$. The result is:

$$\epsilon_{\max} \approx \frac{\delta}{4\pi} + O(\delta^2). \tag{4.2}$$

It is seen that the variation of R with ϵ is quite small, decreasing by 0.061 from $R = 6.93$, when ϵ increased from 0 to the maximum value $\delta/4\pi$. This means that even though subcritical bifurcation to rolls may occur in principle, the interval in R where this is possible is so small that it is unlikely to be seen in an experiment. When $\epsilon > \epsilon_{\max}$, the model predicts negative ϕ, which will be interpreted as the appearance of fully developed chimneys, i.e. regions where the mush has melted away completely. Of course at this point our model breaks down, as it is based on Darcy's law. More sophisticated models, based either on Darcy–Brinkman type equations or a discontinuous model such as that of Worster (1991) must be used. We speculate below that the solution presented here joins a solution branch corresponding to fully developed chimneys at an amplitude given approximately by (4.2).

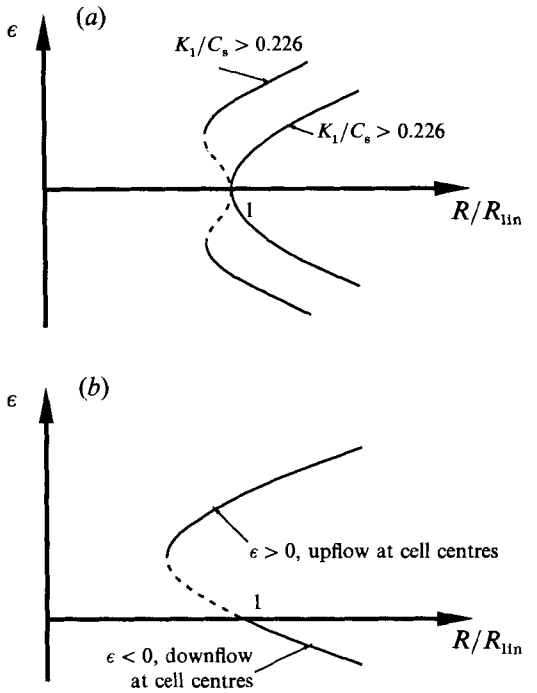

FIGURE 5. Qualitative bifurcation diagrams in the absence of fully developed chimneys. – – –, unstable branches; ——, stable branches, under the assumption of a simple eigenvalue. (*a*) Rolls with hypothetical quintic terms included. (*b*) Hexagons with hypothetical quadratic terms included.

4.2. *Three-dimensional hexagonal convection*

The analogy between the dependency of material parameters on temperature in non-Boussinesq Bénard convection and the coupling between permeability and temperature here, led us to investigate solutions in the form of hexagonal cells. The solutions to first order are given in (3.8), (3.9) and (3.10). As is also the case for non-Boussinesq Bénard convection, the bifurcation is now transcritical, i.e. the first non-zero term in the expansion of R is linear in ϵ, instead of quadratic which was the case for rolls.

The coefficient $R_{1\epsilon}$ never changes sign, so the bifurcation to hexagons is always subcritical. Since $R_{1\epsilon}$ is proportional to the ratio K_1/C_s, the tendency to subcriticality is reduced by increasing C_s and enhanced by increasing K_1, just as for rolls, and for identical reasons. Thus we see that although the nature of the bifurcation is qualitatively different, the same mechanism of the coupling between upflow, melting and flow resistance obtains in three dimensions. In fact, it is stronger, since the convection is not constrained to two dimensions.

Just as for rolls, the finite-amplitude solutions predict a negative solid fraction if ϵ is taken too large. Using equations (3.8*c*), (2.6*d*), (3.1*c*) and (2.9*b*) to estimate the maximum value of ϵ that gives a positive solid fraction, we find:

$$\epsilon_{\max} \approx \frac{\delta}{12\pi} + O(\delta^2), \tag{4.3}$$

which is smaller than that for rolls.

Using the same parameter values $\delta = 0.3$, $C_s = 1$, $St = 1$ and $K_1 = 3$, $K_2 = 6$, as in the example for rolls, $\epsilon_{\max} = \delta/12\pi = 0.00796$. Evaluating the expression for R, equation (3.10), it is seen that R is 0.714 below the critical value 6.75 for linear stability

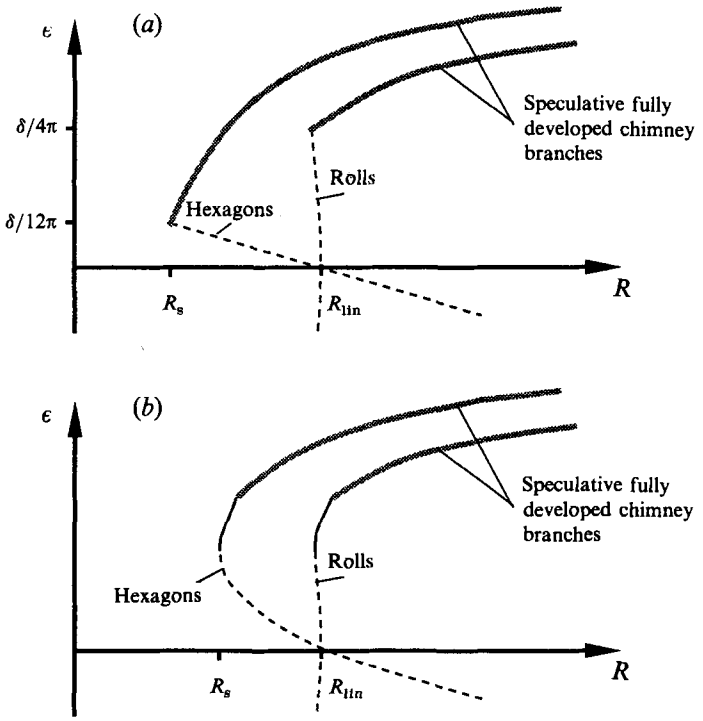

FIGURE 6. Bifurcation diagrams showing qualitatively the appearance of fully developed chimneys. (*a*) – – –, results for subcritical rolls and transcritical hexagons (equations (3.6) and (3.10)). The thicker grey lines are the speculated fully developed chimney branches. (*b*) The same as in (*a*), with qualitative indication of the effects of incorporating higher-order terms. – – –, probably unstable, ——, stable to a general disturbance.

(9.6 below the critical value 45.6 for Ra_D). Thus the interval in R where a bifurcation to hexagons is possible is significant, and may be detectable in an experiment.

4.3. *Speculations on the bifurcation structure*

Our analysis establishes the local bifurcation structure, but is limited for two reasons. First, fundamental properties of sub- and transcritical bifurcations, Iooss & Joseph (1980), show that those branches for which ϵ is a decreasing function of R are probably unstable. Since the mechanism leading to unstable branches is firmly established, they presumably become stable once the highly destabilizing mechanism of remelting due to upflow is inhibited. There are two plausible mechanisms that lead to stable solutions: 'snap through' transitions to either high-amplitude stable states or to fully-developed chimneys.

This first possibility is sketched in figure 6(*b*), where the possible effect of including higher-order terms in the solution is given qualitatively. Figure 5(*a*) shows the effect of computing the quintic terms in the expansion in ϵ for rolls. There is no significant effect for $K_1/C_s < 0.226$, as rolls are supercritical and stable. However, for $K_1/C_s > 0.226$, higher-order terms may stabilize these solutions if the curvature is such that the knee of the curve is below $\epsilon_{max} \approx \delta/4\pi$.

Similarly, figure 5(*b*) shows the possible structure for hexagons. We show the possibility of two branches, representing upflow and downflow in the centres of the cells, respectively, with upflow stable above the turning point, and downflow stable. General considerations (see e.g. Joseph 1971) establish this as a plausible structure. By

computing the quadratic terms in the expansion of R for hexagons, the solution branches would become parabolae and, again, if the second-order terms are large enough, the branch could turn at an amplitude ϵ below $\epsilon_{\max} \approx \delta/12\pi$.

For either rolls or hexagons the solutions would be stable above the turning point and possible to realize in an experiment. These solutions would thus exhibit finite variations in solid fraction, with upflow at locations with low volume fraction, but with a non-zero solid fraction everywhere. The computation of these higher-order terms requires extensive algebra, and remains a topic for further work. In addition to the question of existence of stable solutions due to higher-order terms in the expansion in ϵ, there is also the question of the relative stability of convective patterns. In analogy with the related problem of non-Boussinesq Rayleigh–Bénard convection, it is necessary to establish whether rolls are stable with respect to hexagons, and vice-versa. These calculations also represent a topic for further study.

Our second scenario for what happens to the unstable branches is that nothing moderates the melting and reduced flow resistance in upflow regions until the solid disappears. This is what happens in a fully developed chimney. Figure 6(*a*) illustrates this in a qualitative way. Although our model breaks down at that point, we take the bold step of trusting our solutions up to $\phi = 0$, and take that as the point of transition to chimneys, as explained above. If chimneys are stable, the solution branch should turn forward as shown.

If the speculation is accepted, one specific result that can be obtained here is the extent of the R interval, $R_{\rm lin} - R_{\rm s}$, where subcritical bifurcations to chimneys are possible. For the hexagon solutions this can be estimated from (4.3) and (3.10) to be

$$R_{\rm lin} - R_{\rm s} \approx \frac{1}{12\pi}\left(\tfrac{136}{9} + \tfrac{3}{2}\pi^2\right)\frac{K_1\delta}{C_{\rm s}} = 0.79\frac{K_1\delta}{C_{\rm s}}. \tag{4.4}$$

The corresponding expression for rolls gives $R_{\rm lin} - R_{\rm s} = O(\delta^2)$, i.e. smaller by a factor of δ. Consequently, as indicated in figure 6(*a*), the hexagon branch reaches significantly lower values of R than the roll branch. Our calculations then suggest that a stable fully developed chimney exists at much lower values of R for hexagons than for rolls, showing a preference to form hexagons, at least in the range $R_{\rm s} < R < R_{\rm lin}$.

4.4. *Relationship to experiments*

The results above indicate that the transition to chimney convection is nearly always subcritical, but in two-dimensional Hele-Shaw geometries, the subcritical interval in Rayleigh number is so small that it would be difficult to observe. There are several indirect indications that subcritical transitions do occur, the most compelling of which was reported by Hellawell (1987) in which the mush/melt boundary was disturbed with a pipette. Chimneys failed to form when fine holes were drilled in the mush with the pipette. On the other hand, when fluid was actually withdrawn through the pipette, chimneys invariably formed. These observations are consistent with a subcritical bifurcation, triggered by finite-amplitude upward velocity disturbances. Clearly, in the cases where chimneys were suppressed, the level of disturbances must still have been large enough for linearly unstable modes to be triggered.

Sample & Hellawell (1984), among others, have argued that chimney formation is inherently dependent on processes at the mush–liquid interface. Our analysis shows that this need not be the case, since we have clearly identified a mechanism based on internal convection alone. Tait & Jaupart (1992) have shown that the horizontal lengthscale of the chimneys is much larger than the lengthscale of the thermo-solutal plumes that typically appear owing to the boundary-layer instability. In the present

context it is plausible to view the appearance of chimneys as a subcritical bifurcation which may well be triggered by finite-amplitude disturbances from the plumes above the mush. Once the bifurcation has been triggered though, the bifurcated solution does not depend on details of the initial disturbance, and the properties of chimneys may still be determined primarily by processes taking place inside the mush instead of at the mush–liquid interface.

The possibility of stable downflow at hexagonal cell centres, as suggested by the supercritical $\epsilon < 0$ branch in figure 5(*b*), seems to have strong support in the recent experiments by Tait *et al.* (1992). These were designed with a much lower cooling rate than previous experiments, which probably gave instabilities more time to grow before the background temperature and the mush thickness had changed appreciably. Under one set of conditions, they found that the mush was completely flat and smooth until it reached a thickness of about 1.5 cm. Soon after this a cellular pattern appeared, which consisted of narrow straight channels meeting at junctions. This pattern was characterized as hexagonal by counting the average number of branches meeting at junctions, and measuring average cell area and relating it to side lengths. The lengthscale of the hexagonal cells appears to scale with the depth of the mush. Chimneys were found to evolve from a focusing of the convection at the channel junctions and a freezing over of the channels themselves.

These remarkable findings establish fairly unequivocally that the convection in buoyantly unstable mushy zones is hexagonal, and therefore, by inference, transcritical. While this general fact is in agreement with the calculations given here, the experiments show a strong tendency for upflow along the boundaries (the branch $\epsilon < 0$ in figure 5*b*), while our theory predicts the first unstable branch to be upflow in the centres ($\epsilon > 0$ in figure 5*b*). The experimental tendency for upflow along boundaries appears to be robust, occurring in all the experiments in which hexagons are clearly observed (Tait, private communication). The differences between theory and experiment must for the moment remain unresolved but could be due to several factors, including differences in boundary conditions, limitations of our simplified isotropic continuum model for the mush, the relative stability of different branches to other patterns, the intrinsic time-dependent nature of the experiments, etc. At this stage, both the experimental study of hexagonal mush convection and nonlinear theories are just beginning, and many of these issues remain to be studied.

Some of these issues can be addressed through an analysis of the stability of the different branches. This would probably require a higher-order hexagon solution and much more involved calculations, which have not been attempted here. It can be anticipated though that owing to the multiplicity of the eigenvalue at $R = R_{\mathrm{lin}}$ (allowing both rolls and hexagons), the supercritical $\epsilon < 0$ branch will be unstable (Brattkus & Davis 1988). However, if the multiplicity of the eigenvalue for some reason is removed, the $\epsilon < 0$ branch would be stable, as indicated in figure 5(*b*). Joseph (1971) has shown that this is the case in layers of finite horizontal extent. Since the problem of a fluid layer of infinite extent is always an approximate description of a layer of large but finite aspect ratio, the question is how large this aspect ratio must be for this effect to determine the pattern. Clearly, more complete analyses of these possibilities, together with more careful experiments in which controlled disturbances are introduced, are needed to resolve many of these issues and speculations.

The authors would like to thank Professors Grae Worster and Stephen Davis for helpful comments. GMH acknowledges the support of the US Department of Energy, Office of Basic Energy Sciences.

REFERENCES

BRATTKUS, K. & DAVIS, S. H. 1988 Cellular growth near absolute stability. *Phys. Rev.* B **38**, 11452–11460.

BUSSE, F. H. 1967 The stability of finite amplitude cellular convection and its relation to an extremum principle. *J. Fluid Mech.* **30**, 625–649.

CHAR, B. W., GEDDES, K. O., GONNET, G. H., LEONG, B. L., MONAGAN, M. B. & WATT, S. M. 1991 *Maple V Library Reference Manual.* Springer.

CHEN, C. F. & CHEN, F. 1991 Experimental study of directional solidification of aqueous ammonium chloride solution. *J. Fluid Mech.* **227**, 567–586.

COPLEY, S. M., GIAMEI, A. F., JOHNSON, S. M. & HORNBECKER, M. F. 1970 The origin of freckles in unidirectionally solidified castings. *Metall. Trans.* **1**, 2193–2205.

FELICELLI, S. D., HEINRICH, J. C. & POIRIER, D. R. 1991 Simulation of freckles during vertical solidification of binary alloys. *Metall. Trans.* **22B**, 847–859.

FOWLER, A. C. 1985 The formation of freckles in binary alloys. *IMA J. Appl. Maths* **35**, 159–174.

GLICKSMAN, M. E., CORIELL, S. R. & MCFADDEN, G. B. 1986 Interaction of flows with the crystal–melt interface. *Ann. Rev. Fluid Mech.* **18**, 307–335.

HELLAWELL, A. 1987 Local convective flows in partly solidified alloys. In *Structure and Dynamics of Partially Solidified Systems* (ed. D. E. Loper). Martinus Nijhoff.

HILLS, R. N., LOPER, D. E. & ROBERTS, P. H. 1983 A thermodynamically consistent model of a mushy zone. *Q. J. Mech. Appl. Maths* **36**, 505–539.

HOMSY, G. M. & SHERWOOD, A. E. 1976 Convective instabilities in porous media with through flow. *AIChE J.* **22**, 168–174.

HUPPERT, H. 1990 The fluid mechanics of solidification. *J. Fluid Mech.* **212**, 209–240.

IOOSS, G. & JOSEPH, D. D. 1980 *Elementary Stability and Bifurcation Theory.* Springer.

JOSEPH, D. D. 1971 Stability of convection in containers of arbitrary shape. *J. Fluid Mech.* **47**, 257–282.

NEILSON, D. G. & INCROPERA, F. P. 1993 Effect of rotation on fluid motion and channel formation during unidirectional solidification of a binary alloy. *Intl J. Heat Mass Transfer* **36**, 489–505.

PALM, E., WEBER, J. E. & KVERNVOLD, O. 1972 On steady convection in a porous medium. *J. Fluid Mech.* **54**, 153–161.

SAMPLE, A. K. & HELLAWELL, A. 1984 The mechanisms of formation and prevention of channel segregation during alloy solidification. *Metall. Trans.* A **15**, 2163–2173.

SARAZIN, J. R. & HELLAWELL, A. 1988 Channel formation in Pb–Sn, Pb–Sb, and Pb–Sn–Sb alloy ingots and comparison with the system NH_4Cl–H_2O. *Metall. Trans.* **19**A, 1861–1871.

TAIT, S., JAHRLING, K. & JAUPART, C. 1992 The planform of compositional convection in a mushy layer. *Nature* **359**, 406.

TAIT, S. & JAUPART, C. 1992 Compositional convection in a reactive crystalline mush and melt differentiation. *J. Geophys. Res.* **97**(B5), 6735–6756.

WOODING, R. 1960 Rayleigh instability of a thermal boundary layer in flow through a porous medium. *J. Fluid Mech.* **9**, 183.

WORSTER, M. G. 1991 Natural convection in a mushy layer. *J. Fluid Mech.* **224**, 335–359.

WORSTER, M. G. 1992 Instabilities of the liquid and mushy regions during solidification of alloys. *J. Fluid Mech.* **237**, 649–669.